

## Multiscale seamless domain method for linear elastic and steady temperature problems

\*Y. Suzuki<sup>1</sup>

<sup>1</sup> Department of Mechanical Sciences and Engineering, Tokyo Institute of Technology, Japan.

\*Corresponding author: ysuzuki@ginza.mes.titech.ac.jp

### Abstract

A new meshfree numerical analysis, termed the seamless domain method (SDM), is applied in a multiscale technology. The SDM requires only coarse-grained points and does not need a stiffness equation, mesh, grid, cell, or element. The SDM is composed of two analyses. The first is a microscopic analysis of local simulation domain to obtain shape functions for interpolation of dependent-variable distributions and influence coefficients for calculation of interaction between the points. These allow an SDM solution to represent a heterogeneous material without homogenization. The second step is a macroscopic analysis of a seamless global domain without mesh or grid. Various numerical examples illustrated that the method worked out both steady temperature fields and linear elastic fields. Every SDM solution using only a few hundreds of points was as accurate as that from conventional finite element analysis using more than 300 thousands of node points.

**Keywords:** Multiscale, Meshfree, Non-homogeneous media, Linear elasticity, Steady heat conduction

### Introduction

Most analytical errors of numerical methods involve spatial (and temporal) discretization of a governing equation. Although the discretization in itself is a source of calculation error, conventional numerical techniques cannot produce an approximate solution without spatial division for simulation fields. Although modeling and analyzing the fields with fine node layout (a small mesh) can greatly reduce the error, a large calculation cost is required. In the conventional discretization, so-called shape functions interpolate dependent-variable distributions from the variable values at neighboring points such as nodes and grid points. The error is strongly associated with the precision of interpolating functions. Polynomial functions are generally used for interpolation but the simple functions cannot express a sufficiently smooth variable distribution. Especially in structural analyses, a coarse analytical model often causes problems of shear locking [Wang D et al. (2006); Li S et al. (2000)] and hourglass deformation [Joldes GR et al. (2008)] in conventional finite element methods (FEMs). In general, a variable profile in each finite-element mesh does not obey governing equations because types of shape functions are determined almost regardless of the type of the equations. Additionally, the dependent-variable gradients are discontinuous on grid lines, interfaces between meshes, and interfaces between control volumes. This is because the variable distribution is interpolated from only variable values at nodes in the mesh. Even multiscale FEMs [Chua J et al. (2008); Ilic S et al. (2009)] and multiscale finite volume methods [Jenny P et al. (2004); Lunati I and Jenny P (2006)] cannot generate a continuous variable gradient throughout the field. The above problems can occur when analyzing either a homogeneous field or a heterogeneous field.

There is another demand for multiscale analysis that can model and analyze heterogeneous materials quickly at low computational cost. Heterogeneous materials, such as alloyed metals, plywood, reinforced concrete, and advanced composite structures have been used in many different fields. Composites are composed of multiple constituents and have different physical or chemical properties from the individual components. Although the composite materials can be optimally designed for different purposes in accordance to the use and application, the mechanical, thermal, and electromagnetic tendencies are quite difficult to estimate without a lot of experiments. High-precision numerical analysis that can precisely predict the properties of the composites without performing any experiments would shorten a product development period. Therefore, multiscale schemes, such as homogenization method [Kaczmarczyk Ł et al. (2010)], multiscale FEM [Chua J et al. (2008); Ilic S et al. (2009)], and multiscale finite volume method [Jenny P et al. (2004); Lunati I and Jenny P (2006)], coupling macroscopic and microscopic models are necessary to achieve both high analytical accuracy and low computational cost. However, as mentioned above, these conventional techniques cannot give an exact solution satisfying a governing equation everywhere.

A new meshfree multiscale analysis is developed here to overcome all the above problems [Suzuki Y et al. (2014)]. The scheme is termed the seamless domain method (SDM) because a global field (the entire structure) is modeled as a “seamless” simulation domain that has no element, mesh, or grid. Although the SDM model has only a small number of coarse-grained points (CPs), the solution can represent a heterogeneous material with microscopic constituents without homogenization. Instead of spatial discretization, a local domain (i.e., a part of the global domain) is analyzed before conducting the global analysis. This enables dependent-variable profile in the SDM model to satisfy the governing equations almost perfectly throughout the global domain. Additionally, both the variable and its gradient are continuous everywhere.

To investigate the practical efficacy of the proposed scheme, two kinds of fundamental numerical examples were solved by the SDM: a steady temperature field (scalar field); static linear-elastic fields (vector field). Heterogeneous fiber composite materials were analyzed and both the analytical precision and computational time were compared with those of ordinal FEM analysis. In addition, occurrence of shear locking is also investigated in a bending-dominated problem. As a result, every SDM solution using only a few hundreds of points was shear-locking-free and as accurate as that from conventional finite element analysis using more than 300 thousands of node points.

### **Formulation of the seamless domain method (SDM)**

This section illustrates theoretical framework of the SDM. Cartesian vectors and matrices are used throughout the paper. The proposed SDM couples microscopic local domain and microscopic global domain.

- Local analysis that generates interpolating functions and influence coefficient matrix
- Global analysis that provides a macroscopic solution (i.e., dependent-variable values of all coarse-grained points (CPs)) using the influence coefficient matrix, and the microscopic solution from the macroscopic solution using the interpolating functions

In the local analysis, a small domain composed of a few units to several tens of units is analyzed to obtain high-precision interpolating functions and influence coefficients for the second steps. This objective can be achieved with conventional numerical analysis by finely discretizing governing equation(s) of the local domain spatially (and temporally). The second analysis is of the entire global domain that is represented by CPs. Dependent variable at every CP in the global domain can be obtained using the influence coefficients. After that, the detailed information on the local-variable distributions in the global domain is calculated from the CPs' variable values using the interpolation function obtained in the first step.

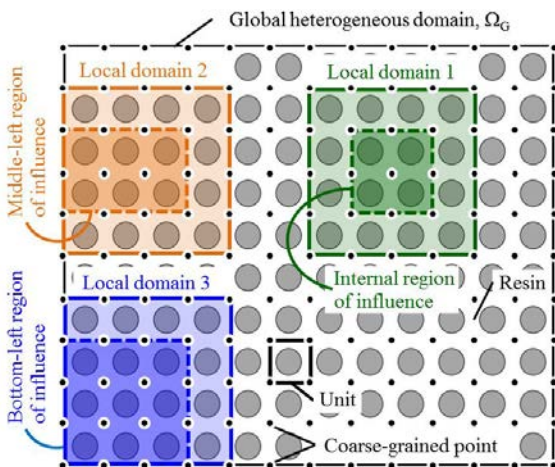
The following subsections will explain the details of each analysis by taking steady temperature problem as an example. Therefore, dependent variable, its gradient, flux, and flow rate are the temperature, temperature gradient, heat flux, and heat flow, respectively.

### Global analysis

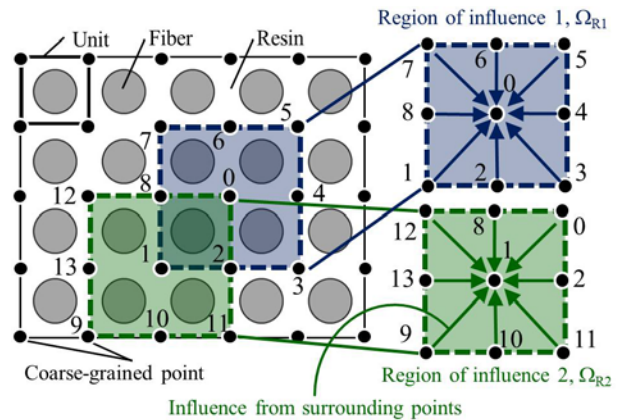
This subsection illustrates how to conduct global analysis with a composite material as an example global domain. As presented in Fig. 1, the composite is assumed to have a perfectly periodic microstructure, called the unit, which has single carbon fiber in the center of the unit.  $\Omega_G (\subset \mathbf{R}^d)$  is a  $d$ -dimensional ( $d = 2$  in this example) global domain whose boundary is  $\Gamma_G$ . The global analysis of the entire composite structure is represented by CPs that are shown as black circles in Fig. 1. The CPs endowed with temperature as a dependent variable are placed at four corners of each unit in this example, which can significantly reduce the number of degrees of freedom (DOF) in comparison with an exact FEM domain that models fiber and polymer separately.

Figure 2 presents a partial magnified image of Fig. 1. A red dashed frame encircling CPs 1–8 is defined as a “region of influence”,  $\Omega_{R1}$ , where neighboring CPs interact with each other. At first, temperature distribution in the red area is calculated. Let us consider a case where temperature at CP 0 is unknown and temperatures at all the CPs remaining in the red frame (i.e., CPs 1–8) are known. The  $m$  CPs ( $m = 8$  in this case) denoted  $\mathbf{u}_{(m)}^R$  on the region's boundary  $\Gamma_{R1}$  and the temperature vector on these CPs is denoted

$$\mathbf{u}_{(m)}^R = (u_1^R \quad \dots \quad u_m^R)^T \text{ on } \Gamma_{R1}, \quad (1)$$



**Figure. 1** Heterogeneous global domain (fiber composite) that is assumed to have a perfectly periodic microstructure



**Figure. 2** Regions of influence in partial magnified image of the heterogeneous global domain as shown in Fig. 1

where  $u_i^R$  is temperature at CP  $i$ . The superscript ‘‘T’’ refers to the transposition of a matrix or vector. Unless heat enters from outside the system, the correct temperature contour in the blueframe can be calculated from the temperature profile on the frame. However, there are infinitely many points and temperature DOFs on the frame, and this estimation approach is thus unrealistic. Therefore, the temperature distribution in the blue frame is estimated referring to temperatures at CPs 1–8.

$$u_{(m)}(\mathbf{x}) = \mathbf{N}_{(m)}(\mathbf{x})\mathbf{u}_{(m)}^R \text{ in } \Omega_{R1}, \quad (2)$$

where  $u_{(m)}(\mathbf{x})$  is temperature at position  $\mathbf{x} = (x, y)^T \in \Omega_{R1}$  and  $\mathbf{N}_{(m)}$  is a special interpolating function matrix derived in local analysis. Details of the local analysis will be illustrated in the next subsection. The number of CPs,  $m$  need not necessarily be 8. A sufficient number of reference CPs gives a true temperature distribution. Even if the global domain is not homogeneous, there is no necessity to separately model the microscopic constituents but the structural heterogeneity is exactly taken into account. After obtaining the temperature distribution in the blue frame,  $u_{(m)}(\mathbf{x})$ , temperature at CP 0 is thus determined by substituting  $\mathbf{x} = \mathbf{0}$  into Eq. 2.

$$u_0^R = u_{(m)}(\mathbf{0}) = \mathbf{N}_{(m)}(\mathbf{0})\mathbf{u}_{(m)}^R = \mathbf{a}_{(m)}\mathbf{u}_{(m)}^R \quad (3)$$

where

$$\mathbf{a}_{(m)} = \mathbf{N}_{(m)}(\mathbf{0}) = (a_1 \quad \cdots \quad a_m) \quad (4)$$

is a influence coefficient matrix. As it is, however, the global domain is spatially discretized by the blue frame and becomes a patchy domain having many seams. There is no guarantee that temperature and its gradient on the seam (i.e., frame) are continuous. To eliminate the seam, we should follow the procedure explained below. Temperature at CP 1 is estimated referring to the remaining CPs in the green dashed frame (i.e., CPs 0, 2, 8–13 in Fig. 2) using  $\mathbf{a}_{(m)}$  in Eq. 4. It is of importance that both the blue frame ( $\Omega_{R1}$ ) and green frame ( $\Omega_{R2}$ ) contain CPs 0, 1, 2, 8. These shared CPs works for making the temperature contour in the shared region ( $\Omega_{R1} \cap \Omega_{R2}$ ) interpolated referring to temperature at CPs 1–8 in the blue frame correspond with that interpolated from CPs 0, 2, 8–13 in the green frame. When the shared region has a sufficient number of shared CPs, the two temperature distributions match exactly. As this improves continuity of the temperature and its gradient on the shared frame greatly, the shared frame is no longer a seam. By describing frames centered at each of the CPs, the global domain is filled with shared regions. There is no region or seam belonging to an unshared and isolated frame, and the global domain finally becomes ‘‘seamless’’ and has continuous distributions of temperature and its gradient satisfying the governing equation(s) almost exactly.

Note that the SDM calculates temperature at a CP referring to temperature at surrounding CPs. There is no necessity to formularize and solve a stiffness equation (i.e., nodal equation of equilibrium) that determines the relation between nodal heat flow and the nodal temperature. When  $n$  CPs represent a two-dimensional global domain,  $\Omega_G$ , there is  $n$  DOFs in  $\Omega_G$ . The vector including all the CPs’ temperature in  $\Omega_G$ ,  $\mathbf{u}_{(n)}^G$ , has  $n$  components

$$\mathbf{u}_{(n)}^G = (u_1^G \quad \cdots \quad u_n^G)^T \text{ in } \Omega_G. \quad (5)$$

We can formularize the same number of relational expressions between the temperature of the center CP and those of surrounding CPs like Eq. 3 as that of the components of  $\mathbf{u}_{(n)}^G$ . Consequently, the temperatures of all the CPs in  $\Omega_G$ ,  $\mathbf{u}_{(n)}^G$ , can be determined uniquely. The  $\mathbf{u}_{(n)}^G$  satisfies the following algebraic equations.

$$\mathbf{a}_{(n)}^G \mathbf{u}_{(n)}^G = \mathbf{u}_{(n)}^G, \quad (6)$$

where matrix  $\mathbf{a}_{(n)}^G$  is established by assembling all the influence coefficient matrices,  $\mathbf{a}_{(m)}$ .  $\mathbf{a}_{(n)}^G$  is a band matrix whose rows and columns are the same as the number of the CPs,  $n$  :

$$\mathbf{a}_{(n)}^G = \begin{bmatrix} a_{1,1}^G & a_{1,2}^G & \cdots & \cdots & a_{1,n}^G \\ a_{2,1}^G & \ddots & \cdots & \cdots & \vdots \\ \vdots & \cdots & a_{i,j}^G & \cdots & \vdots \\ \vdots & \cdots & \cdots & \ddots & \vdots \\ a_{n,1}^G & \cdots & \cdots & \cdots & a_{n,n}^G \end{bmatrix}, \quad (7)$$

where  $a_{i,j}^G$  is the component in the  $i$ -th row and  $j$ -th column of  $\mathbf{a}_{(n)}^G$ . By imposing boundary conditions into Eq. 6, the solution of  $\mathbf{u}_{(n)}^G$  is calculated uniquely. For example, let us consider a Dirichlet boundary problem where a CP's temperature  $u_i^G$  is given and the other temperatures are unknown. At first, all the unknown temperatures on the right side of Eq. 6 are transposed to the left side:

$$\begin{bmatrix} a_{1,1}^G - 1 & a_{1,2}^G & \cdots & \cdots & \cdots & \cdots & a_{1,n}^G \\ \vdots & \ddots & \cdots & \cdots & \cdots & \cdots & \vdots \\ a_{i-1,1}^G & \cdots & a_{i-1,i-1}^G - 1 & a_{i-1,i}^G & a_{i-1,i+1}^G & \cdots & a_{i-1,n}^G \\ a_{i,1}^G & \cdots & a_{i,i-1}^G & a_{i,i}^G & a_{i,i+1}^G & \cdots & a_{i,n}^G \\ a_{i+1,1}^G & \cdots & a_{i+1,i-1}^G & a_{i+1,i}^G & a_{i+1,i+1}^G - 1 & \cdots & a_{i+1,n}^G \\ \vdots & \cdots & \cdots & \cdots & \cdots & \ddots & \vdots \\ a_{n,1}^G & a_{n,2}^G & \cdots & \cdots & \cdots & a_{n,n-1}^G & a_{n,n}^G - 1 \end{bmatrix} \begin{bmatrix} u_1^G \\ \vdots \\ u_{i-1}^G \\ u_i^G \\ u_{i+1}^G \\ \vdots \\ u_n^G \end{bmatrix} = \begin{bmatrix} 0 \\ \vdots \\ 0 \\ u_i^G \\ 0 \\ \vdots \\ 0 \end{bmatrix}. \quad (8)$$

Subsequently, 1 and 0 are substituted into  $a_{i,i}^G$  and the remaining components in the  $i$ -th row, respectively:

$$\begin{bmatrix} a_{1,1}^G - 1 & a_{1,2}^G & \cdots & \cdots & \cdots & \cdots & a_{1,n}^G \\ \vdots & \ddots & \cdots & \cdots & \cdots & \cdots & \vdots \\ a_{i-1,1}^G & \cdots & a_{i-1,i-1}^G - 1 & a_{i-1,i}^G & a_{i-1,i+1}^G & \cdots & a_{i-1,n}^G \\ 0 & \cdots & 0 & 1 & 0 & \cdots & 0 \\ a_{i+1,1}^G & \cdots & a_{i+1,i-1}^G & a_{i+1,i}^G & a_{i+1,i+1}^G - 1 & \cdots & a_{i+1,n}^G \\ \vdots & \cdots & \cdots & \cdots & \cdots & \ddots & \vdots \\ a_{n,1}^G & a_{n,2}^G & \cdots & \cdots & \cdots & a_{n,n-1}^G & a_{n,n}^G - 1 \end{bmatrix} \begin{bmatrix} u_1^G \\ \vdots \\ u_{i-1}^G \\ u_i^G \\ u_{i+1}^G \\ \vdots \\ u_n^G \end{bmatrix} = \begin{bmatrix} 0 \\ \vdots \\ 0 \\ u_i^G \\ 0 \\ \vdots \\ 0 \end{bmatrix}. \quad (9)$$

By multiplying both sides of Eq. 9 by the inverse of the matrix on the left side of Eq. 9, we can determine all the components of  $\mathbf{u}_{(n)}^G$ . After solving the above equation, local-temperature

distributions can be easily obtained by interpolating from  $\mathbf{u}_{(n)}^G$  using  $\mathbf{N}_{(m)}(\mathbf{x})$  in Eq. 2. Although the above illustration shows how to solve a Dirichlet boundary problem, the SDM can also solve Neumann boundary problems and mixed boundary problems. Note that the number of reference CPs in the region of influence,  $m$ , is arbitrary in Eqs. 1–4.

### Local analysis

Before conducting global analysis, local analysis is done to calculate the interpolating function matrix  $\mathbf{N}_{(m)}$  in Eq. 2 and influence coefficient matrix  $\mathbf{a}_{(m)}$  in Eq. 4. This objective can be achieved by analyzing a local domain  $\Omega_L$  ( $\subset \mathbf{R}^d$ ) with boundary  $\Gamma_L$  that is extracted from the global domain,  $\Omega_G$ , as shown in Fig. 3. In this case,  $\Omega_L$  is composed of 16 units. Although the local analysis is done employing the traditional FEM, other conventional numerical techniques can be also used. By dividing  $\Omega_L$  into fine meshes having a sufficient number of nodes,  $\mathbf{N}_{(m)}$  and  $\mathbf{a}_{(m)}$  for each region of influence  $\Omega_R$  can be obtained.

Let us illustrate how to construct  $\mathbf{N}_{(m)}$  and  $\mathbf{a}_{(m)}$  for the internal region of influence. As depicted in Fig. 3(a),  $\Omega_L$  includes the internal region,  $\Omega_R$ , composed of four units ( $\Omega_R \subset \Omega_L$ ). The  $\Omega_R$  has  $m$  CPs on the edge,  $\Gamma_R$ , and another CP (CP 0) in the center. Figure 3(a) illustrates a case where  $m$  is equal to 8. In the global analysis, temperature profile in the  $\Omega_R$  is determined referring to the temperature values at the  $m$  CPs using  $\mathbf{N}_{(m)}$ . Encircling  $\Omega_R$  with the outer 12 units is termed the oversampling method [Henning P et al. (2013); Efendiev Y et al. (2013)]. It is known that oversampling reduces boundary effect on  $\Omega_R$ . The dimension of the domain,  $d$ , is equal to 2 in this case. The  $m$  CPs denoted  $\mathbf{u}_{(m)}^R$  in Eq. 1 and the  $m$  nodes denoted  $\mathbf{u}_{(m)}^L$  are put on the region's boundary  $\Gamma_R$  and the local domain's boundary  $\Gamma_L$ , respectively. The temperature vector  $\mathbf{u}_{(m)}^L$  on those points are denoted

$$\mathbf{u}_{(m)}^L = (u_1^L \quad \dots \quad u_m^L)^T \text{ on } \Gamma_L. \quad (10)$$

As shown in Fig. 3, a Dirichlet boundary is put on  $\Gamma_L$  so that the  $\Gamma_L$  has given linear temperature profile. The temperature of the center CP 0 and that at an arbitrary point  $\mathbf{X}$  ( $\in \Omega_R$ ) are denoted  $u_0^R$ ,

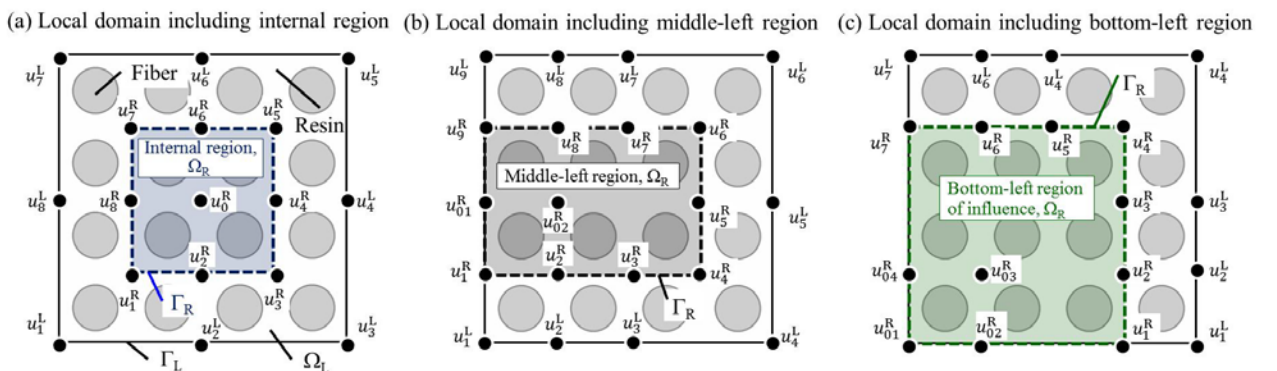


**Figure 3. Layout of coarse-grained points (CPs) in local domains for the SDM analysis: (a) shows local domain including the internal region of influence; (b) shows local domain including the middle-left region; (c) shows local domain including the bottom-left region**

$u_{(m)}(\mathbf{x})$ , respectively. The objective of the local analysis is to calculate the relations between  $\mathbf{u}_{(m)}^L$  and the other temperatures  $u_0^R$  and  $u_{(m)}(\mathbf{x})$ :

$$\begin{aligned} u_0^R &= \mathbf{A}_{(m)}^R \mathbf{u}_{(m)}^L \\ u_{(m)}(\mathbf{x}) &= \mathbf{A}_{(m)}(\mathbf{x}) \mathbf{u}_{(m)}^L \end{aligned} \quad (11)$$

All the entries of  $\mathbf{A}_{(m)}^R$  and  $\mathbf{A}_{(m)}(\mathbf{x})$  can be derived from only a single analysis of local domain. The  $\mathbf{u}_{(m)}^L$  and  $\mathbf{u}_{(m)}(\mathbf{x})$  are expressed in the form

$$\begin{aligned} \mathbf{u}_{(m)}^L &= (\mathbf{A}_{(m)}^R)^{-1} \mathbf{u}_{(m)}^R \\ u_{(m)}(\mathbf{x}) &= \mathbf{A}_{(m)}(\mathbf{x}) (\mathbf{A}_{(m)}^R)^{-1} \mathbf{u}_{(m)}^R = \mathbf{N}_{(m)}(\mathbf{x}) \mathbf{u}_{(m)}^R \end{aligned} \quad (12)$$

where

$$\mathbf{N}_{(m)}(\mathbf{x}) = \mathbf{A}_{(m)}(\mathbf{x}) (\mathbf{A}_{(m)}^R)^{-1}, \quad (13)$$

is the interpolating function matrix that was stated in the previous subsection. When the  $\Omega_L$  has a sufficient number of nodes,  $\mathbf{N}_{(m)}(\mathbf{x})$  provides accurate temperature profile. By substituting  $\mathbf{x}=\mathbf{0}$  into  $\mathbf{N}_{(m)}(\mathbf{x})$  in Eq. 12, the  $\mathbf{a}_{(m)}$  can be calculated like Eqs. 3 and 4. Equation 3 shows that  $u_0^R$  can be written as a linear combination of  $\mathbf{a}_{(m)}$  and  $\mathbf{u}_{(m)}^R$ . Each component of  $\mathbf{a}_{(m)}$  is the influence of a surrounding CP on CP 0 as shown by the arrows in Fig. 2. An increase in the number of CPs  $m$  improves the calculation accuracy of  $u_0^R$ .

The above illustration shows how to make the internal region of influence. Respectively different  $\mathbf{N}_{(m)}$  and  $\mathbf{a}_{(m)}$  need to be prepared for the other outer regions depicted in Figs. 3(b) and (c) because the outer regions are adjacent to a free edge and receive a boundary effect through one or more aspects of the region. For instance, 2-by-3 units located at the left side of the local domain are defined as the middle-left region of influence. In this region, unknown temperatures at CPs 01 and 02,  $u_{01}^R, u_{02}^R$ , are calculated referring to temperatures at 9 CPs (CPs 1–9). Another region located at the corner of the local domain has 3-by-3 units as shown in Fig. 3(c). In the region, temperatures at CPs 01–04,  $u_{01}^R, u_{02}^R, u_{03}^R, u_{04}^R$ , are estimated referring to temperatures at 7 CPs (CPs 1–7).  $\mathbf{N}_{(m)}$  and  $\mathbf{a}_{(m)}$  of these outer regions can be obtained in a similar way to those of the internal region. Constructing respective  $\mathbf{N}_{(m)}$  and  $\mathbf{a}_{(m)}$  for each region enables the SDM solution to take the boundary effect into account. In preparing the outer regions, we only have to move the CPs so that the region has contact with the local domain's boundary as shown in Figs. 3(b) and (c). In addition, both the number and arrangement of CPs in the local domain are arbitrary in Eqs. 10–13 and Figs. 1–3. Consequently, all the regions can be constructed from a result of single local analysis. In other words, there is no necessity to conduct FEM analysis of the local domain twice or more [Suzuki Y et al. (2014)].

## Numerical examples

### Outline

Numerical example problems for testing the practical efficacy of the SDM technique are outlined. To investigate the simulation accuracy and calculation cost, several heterogeneous fields such as steady temperature field and linear elastic fields are analyzed employing the following two numerical techniques:

- the SDM scheme with quadrangular regions of influence, and
- the conventional FEM analysis with four-node linear isoparametric meshes.

It is mathematically guaranteed that an FEM solution converges to exactly correct one when the finite-element mesh is infinitesimally fine. The two methods are compared in terms of analytical accuracy and computational cost. In all the examples, local analyses of the SDM are conducted employing a traditional FEM. The target heterogeneous fields are fiber composite materials that have carbon fibers in polymer matrix as depicted in Figs. 4 and 5. The composites, which have a huge number of fibers about 5–15  $\mu\text{m}$  in diameter in the polymer matrix, have been used as a structural material in aircraft and aerospace components because they exhibit superior mechanical properties, higher fatigue strength characteristics, lower mass density, and higher corrosion resistance than conventional metallic materials. A heterogeneous material is assumed to have a perfectly periodic microstructure, termed the unit, which has a carbon fiber as shown in Figs. 4 and 5.

In local analysis of the SDM, a small local domain composed of 4-by-4 units extracted from the entire global field is analyzed to calculate an interpolation function matrix  $\mathbf{N}_{(m)}$  in Eq. 2 and influence coefficient matrix  $\mathbf{a}_{(m)}$  in Eq. 3 for each region of influence. For the numerical examples, we need prepare one kind of internal region of influence and 8 types of outer regions for the subsequent global analysis. The internal region represents part of the global domain that is located inside the global domain and not adjacent to the global domain's boundary. Figure 3(a) illustrates how to construct  $\mathbf{a}_{(m)}$  and  $\mathbf{N}_{(m)}$  for the internal region. The 2-by-2 units that are located at the center of the local domain and enclosed in the dashed frame are targeted as the internal region; the area encircled by the bold frame forms a surrounding region to remove the boundary effect on the target. On the other hand, the other 8 types of regions represent outer parts of the global domain. One or two surfaces of the outer regions are adjoined to the global boundary. In calculating  $\mathbf{N}_{(m)}$

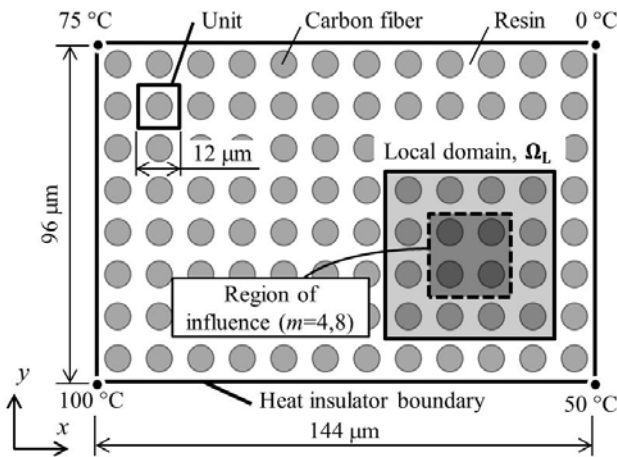


**Figure 4. Fiber composite global domain for the steady temperature example problem**

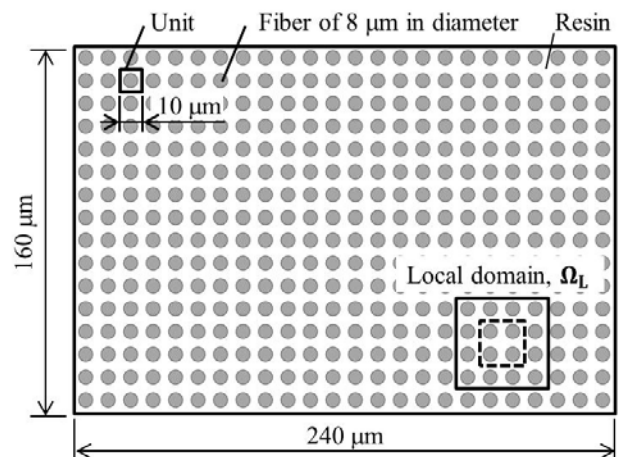


**Figure 5. Heterogeneous global domain for the linear-elastic numerical example**

and  $\mathbf{a}_{(m)}$  for the outer regions, CPs are arranged and the regions of influence are extracted as shown Figs. 3(b) and (c). Once the two regions (i.e., middle-left and bottom-left regions) are constructed, the other six kinds of regions (i.e., middle-right, top-middle, bottom-middle, bottom-right, top-left, and top-right regions) can be easily generated by geometric symmetries. Again, note that all the regions can be prepared from the result of the single local analysis.

After the FEM analysis of the local domain is finished, we move on to the SDM analysis of the global domain. The SDM global field does not require individual fiber and polymer models. Because the heterogeneous material has a periodic unit, the global domain has evenly spaced CPs. After assembling and solving algebraic equations like Eq. 9 to determine dependent-variable values of all CPs,  $\mathbf{u}_{(n)}^G$  in Eq. 5, the variable distribution in the global domain is interpolated from  $\mathbf{u}_{(n)}^G$  using  $\mathbf{N}_{(m)}(\mathbf{x})$  in Eq. 2.

#### *Problem statement for steady-state heat conduction*

A steady temperature heterogeneous field as shown in Fig. 4 is analyzed by the SDM and ordinal FEM. The conditions are: two-dimensional; steady-state. The vector of heat flux, matrix of thermal conductivity, and temperature of an arbitrary point  $\mathbf{x}$  are denoted  $\mathbf{q}(\mathbf{x}) \in \mathbf{R}^2$ ,  $\mathbf{C}(\mathbf{x}) \in \mathbf{R}^{2 \times 2}$ , and  $u(\mathbf{x}) \in \mathbf{R}$ , respectively.

$$\mathbf{q}(\mathbf{x}) = -\mathbf{C}(\mathbf{x})\nabla u(\mathbf{x}), \quad (14)$$

where

$$\mathbf{D}(\mathbf{x}) = \begin{pmatrix} C_{11} & C_{12} \\ C_{21} & C_{22} \end{pmatrix}, \quad (15)$$

$u(\mathbf{x})$  then satisfies the governing equation

$$\mathbf{C}(\mathbf{x})\Delta u(\mathbf{x}) = \mathbf{C}(\mathbf{x})\nabla^2 u(\mathbf{x}) = C_{11} \frac{\partial^2 u(\mathbf{x})}{\partial x_1^2} + C_{22} \frac{\partial^2 u(\mathbf{x})}{\partial x_2^2} = 0 \text{ for } \forall \mathbf{x} = (x, y)^T \in \Omega, \quad (16)$$

throughout the simulation field. If the domain is isotropic and has the same thermal conductivities in the  $x$  and  $y$  axes,

$$C_{11} = C_{22} \neq 0,$$

then

$$\frac{\partial^2 u}{\partial x^2} + \frac{\partial^2 u}{\partial y^2} = 0. \quad (17)$$

As depicted in Fig. 4, Dirichlet boundary conditions are imposed on the target carbon fiber/epoxy resin composite material. The temperatures at top-left, top-right, bottom-left, and bottom-right corners are fixed at 75, 0, 100, and 50 °C, respectively. The outer edge of the global domain except for the four corners is a heat insulation wall. Thermal conductivity coefficients used for the analysis are listed in Table 1.

**Table 1. Thermal conductivity values used in analyses of the examples**

Material	Thermal conductivity [ $\text{W} \cdot \text{m}^{-1} \cdot \text{K}^{-1}$ ]		
	$C_{11}$	$C_{22}$	$C_{12} = C_{21}$
Carbon fiber	500	500	0
Epoxy resin	0.26	0.26	0

In the SDM analysis, we test two cases where  $m = 4$  (Fig. 6(a)) and  $m = 8$  (b).  $m$  is the number of reference CPs for temperature. The local domain,  $\Omega_L$ , is divided into fine finite-element meshes and analyzed with Dirichlet boundary conditions of  $u_1^L, u_2^L, \dots, u_m^L$  on the  $m$  CPs on the boundary of  $\Omega_L$  and  $\Gamma_L$ , to obtain the interpolating function matrix,  $\mathbf{N}_{(m)}(\mathbf{x})$  in Eq. 2, and influence coefficient vector,  $\mathbf{a}_{(m)}$  in Eq. 3.  $\Omega_L$  has 3,649 nodes. The global domain is represented by 59 CPs in the case that  $m = 4$  and 117 CPs in the cases that  $m = 8$ . After constructing and solving algebraic equations like Eq. 9 to determine temperature values of all CPs,  $\mathbf{u}_{(n)}^G$  in Eq. 5, the temperature contours in the global domain is interpolated from  $\mathbf{u}_{(n)}^G$  using  $\mathbf{N}_{(m)}(\mathbf{x})$ . Conversely, in the traditional FEM, fiber and polymer are modeled separately and divided into sufficiently fine meshes (more than 20 thousands of node points).

*Problem statement for linear elasticity*

The static elasticity fields as described in Fig. 7 are analyzed. The conditions are: two-dimensional; static; linear elastic; plane stress. The vectors of stress, engineering strain, and displacement of an arbitrary point  $\mathbf{x}$  ( $\in \Omega$ ) are denoted  $\boldsymbol{\sigma}(\mathbf{x}) \in \mathbf{R}^3$ ,  $\boldsymbol{\varepsilon}(\mathbf{x}) \in \mathbf{R}^3$ , and  $\mathbf{u}(\mathbf{x}) \in \mathbf{R}^2$ , respectively. The constitutive law for the domain can be written in the form

$$\boldsymbol{\sigma}(\mathbf{x}) = \mathbf{D}(\mathbf{x})\boldsymbol{\varepsilon}(\mathbf{x}), \quad (18)$$

where

$$\boldsymbol{\varepsilon}(\mathbf{x}) = \begin{bmatrix} \varepsilon_x \\ \varepsilon_y \\ \gamma_{xy} \end{bmatrix} = \begin{bmatrix} \partial u / \partial x \\ \partial v / \partial y \\ \partial u / \partial y + \partial v / \partial x \end{bmatrix}, \quad (19)$$

and  $u, v$  are displacements in the  $x$  and  $y$  axes at  $\mathbf{x}$ , respectively.

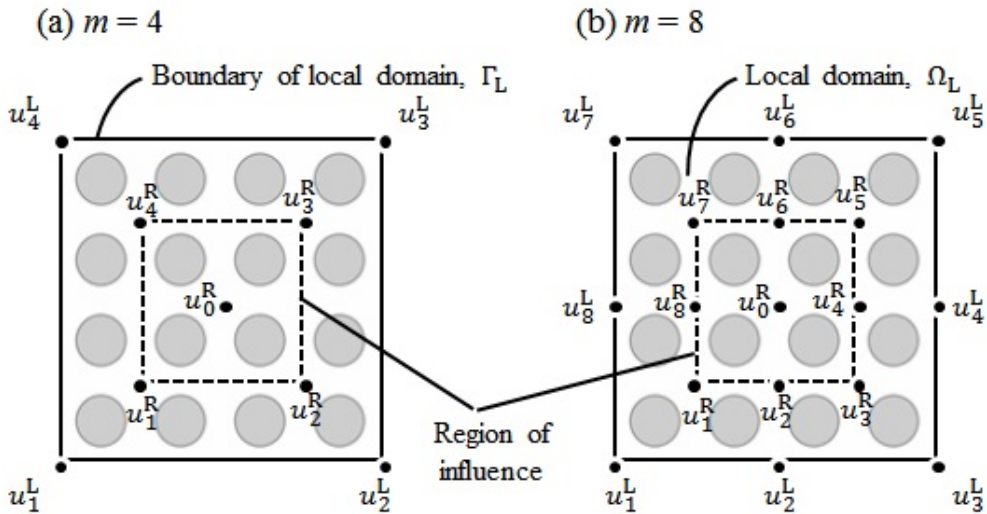


**Figure 6. Layout of coarse-grained points (CPs) in local domains for the SDM analysis: (a) shows the case that  $m = 4$ ; (b) shows the case that  $m = 8$**

**Table 2. Linear elastic properties of the carbon fiber and polyimide resin models [Rupnowski P et al. (2005)]**

Material	Young's modulus in the $x$	Young's modulus in the $y$	Poisson ratio, $\nu_{xy}$
Carbon fiber (T650-35)	13.8 GPa	13.8 GPa	0.37
Polyimide resin (PMR-15)	4.0 GPa	4.0 GPa	0.29

Figure 7 describes three carbon fiber (T650-35)/Polyimide resin (PMR-15) composites consisting of 16-by-24 units which have single fiber in the center under: (a) a uniaxial tensile load; (b) a bending load; (c) a shearing load. Perfect bonding between the fibers and resin matrix is assumed. The elastic properties are listed in Table 2 [Rupnowski P et al. (2005)].

In the example, we test single case where  $m = 8$ . The local domain,  $\Omega_l$ , has 14,864 nodes. Global analysis of the SDM is conducted using  $\mathbf{N}_{(m)}$  and  $\mathbf{a}_{(m)}$  obtained in the local analysis. The three global domains shown in Figs. 7(a)–(c) have the same structure but different boundary conditions are imposed. Each global domain of the SDM is represented by 425 CPs, while more than 300 thousands of nodes are in the FEM model. This is because the SDM global domains do not require individual fiber and polymer models. After constructing and solving algebraic equations like Eq. 9 to determine displacement values of all the CPs,  $\mathbf{u}_{(n)}^G$  in Eq. 5, the displacement distribution in the global domain is interpolated from  $\mathbf{u}_{(n)}^G$  using  $\mathbf{N}_{(m)}(\mathbf{x})$  in Eq. 12.

#### Results for steady-state heat conduction

Figures 8 present the temperature distribution,  $u$ , and temperature gradients,  $\partial u/\partial x$  and  $\partial u/\partial y$ , in the heterogeneous domain. In the traditional FEM, fiber and polymer are modeled separately and divided into sufficiently fine meshes. Therefore, the FEM solutions as depicted in Fig. 8(a) are believed to be exactly correct. Therefore, when the SDM solution (Figs. 8(b) and (c)) accords with the FEM result, calculation error of the SDM is regarded as zero.

A sharp change in temperature from 0 to 100 °C is generated over the global domain. The temperature distribution calculated with the SDM having 59 CPs (Fig. 8(b)) is partially discontinuous. This means that the number of reference CPs,  $m = 4$  is insufficient to give the exact solution. The temperature distributions of the SDM consisting of 117 CPs (Fig. 8(c)) almost completely matches that obtained with the conventional FEM with more than 20 thousands of nodes. Therefore, it is believed that  $m = 8$  is enough for solving the example problem. The contours of the temperature gradient in Fig. 8(c) show that high resolution of localized steep gradients can be

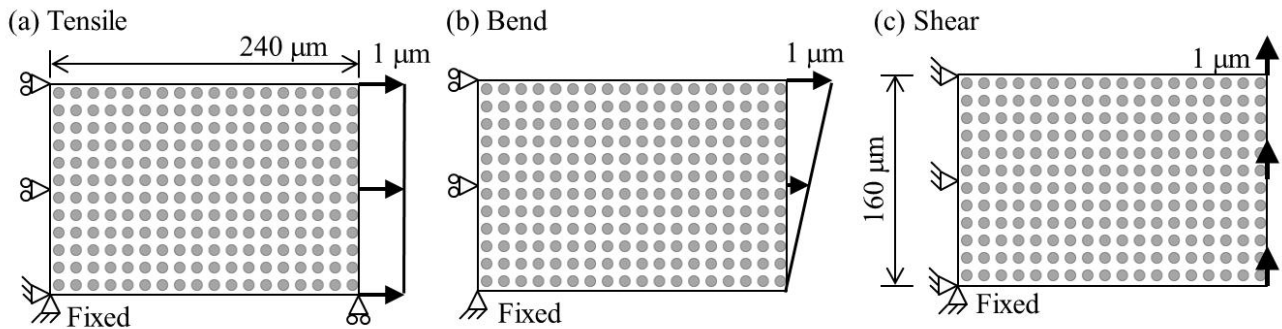


**Figure 7. Three carbon fiber composite structures: (a)–(c) show the analysis model under a uniaxial tensile load, a bending load, and a shearing load, respectively**

achieved by the SDM.

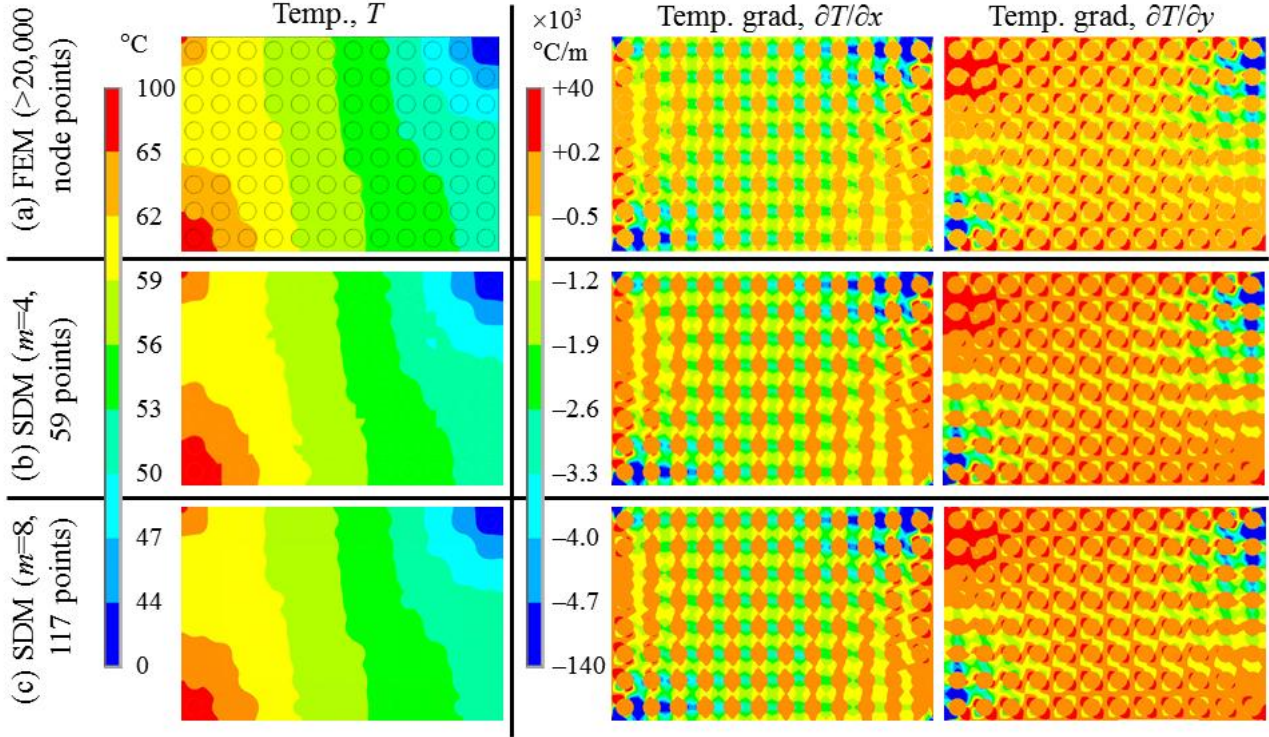


**Figure 8.** Calculated steady-state temperature and temperature gradient distributions in the composite material: (a)–(c) describe the results of FEM with >20,000 nodes, those of the SDM with 59 points ( $m=4$ ), and those of the SDM with 117 points ( $m=8$ ), respectively

**Table 3.** Comparison of analytical accuracies and calculation times

Item	DOF	Average difference in temp.	Average difference in temp. gradient		Total calculation time
			$u$	$\partial u/\partial x_1$	
Symbol		Degree	$\times 10^4$ °C/m		s
Unit		Degree	$\times 10^4$ °C/m		s
FEM	>20,000	0	0	0	8.10
SDM ( $m=4$ )	59	1.35	12.1	6.34	1.12
SDM ( $m=8$ )	117	0.00308	4.42	0.781	1.14

Table 3 gives the average values of the absolute difference in temperature,  $u$ , and that in temperature gradients,  $\partial u/\partial x$  and  $\partial u/\partial y$ , when comparing with the result of the conventional FEM. The average difference in  $u$  over all CPs in the case of 59 CPs ( $m=4$ ) and in the case of 117 CPs ( $m=8$ ) are 1.35, 0.00308 °C, respectively. Although the temperature result for  $m=4$  is not exactly correct in comparison with the temperature difference of 100 °C arising in the global domain, there is no temperature difference at all for  $m=8$ . The average differences in  $\partial u/\partial x$  and  $\partial u/\partial y$  for  $m=8$  are  $4.42 \times 10^4$  and  $0.781 \times 10^4$  °C/m, respectively. These errors are sufficiently small because the maximum temperature gradients of  $\partial u/\partial x$  and  $\partial u/\partial y$  at all CPs are both  $1.40 \times 10^7$  °C/m. As shown in Figs. 15 and 16, employing 117 CPs in the SDM ( $m=8$ ) gives highly continuous distributions of  $\partial u/\partial x$  and  $\partial u/\partial y$  that are almost the same as those of the exact result obtained with the FEM and >20,000 of nodes.

The total computational times are compared in Table 3. The results include the time expended in meshing domains and solving the inverse matrix of matrix in Eq. 9. For the SDM, total computational time of the local and global analyses is presented. In the SDM, increase of the

number of CPs enhances greatly the simulation precision but requires little additional calculation time. The conventional FEM with more than 20 thousands of nodes has 7.1 times the calculation cost of the SDM with 117 CPs in producing a solution as accurate as that of the SDM.

*Results for linear elasticity*

Figure 9 presents calculated displacement and strain contours in the composite models under: (a) a uniaxial tensile load; (b) a bending load; (c) a shearing load. As stated above, all the FEM results in Figure 9 are supposed to give the almost exact solution. Each SDM model is represented by 425 CPs. Therefore, if the SDM result accords with the FEM result, analytical error of the SDM is regarded as zero. As shown in Figs. 9(a)–(c), all the contours of displacement and strain obtained with the SDM are sufficiently continuous and appear to exactly match those obtained with the conventional FEM. Table 4 presents the average values of the absolute difference in displacement over all CPs between the SDM solutions and the FEM solutions. All of the average difference in displacement in the  $x$  axis,  $u$ , and that in the  $y$  axis,  $v$ , are less than  $0.007 \mu\text{m}$ . The three composite materials in Figs. 7(a)–(c) receive respectively different types of loads but the same maximum displacement of  $1 \mu\text{m}$  occurs in them. Therefore, these differences are sufficiently small compared with the maximum displacement in the domain and practically negligible.

As a traditional FEM generally interpolates displacement contour in each mesh from displacement at nodes in the mesh using a simple polynomial function, coarse-mesh layout cannot reproduce a complicated displacement profile. Especially, FEM models with fully integrated first-order quadrangular solid meshes (or hexahedral solid meshes in a case of three-dimensional analysis) tend to overestimate the stiffness in bending-dominated problems. This problem is called shear locking and occurs because a first-order mesh cannot represent a curved surface. However, as shown in Fig. 9(b), employing only 425 CPs in the SDM reproduce smooth bending deformation and does not cause shear locking because the displacement is interpolated by exact functions obtained by the prior analysis of fine-mesh local domain. For the similar reason, the SDM model is free of hourglass deformation. Hourglassing is another major problem of the FEM caused in certain coarse-grained domains. This is zero-energy deformation mode where a mesh deforms without consuming strain energy because all kinds of stresses at each integration point in the mesh are zero.

Table 5 presents comparison of the total computational times required to solve the problems. In giving a solution as accurate as that of the SDM, the conventional FEM requires more than one hundred times the calculation cost of the SDM. As the size of the global domain becomes large, the FEM has huge cost and becomes inefficient. In contrast, the SDM can analyze a large global domain without considerable cost and its competitiveness and effectiveness become higher as the global domain increases in size.

**Table 4. Differences in displacement between the SDM and the FEM when analyzing three FRP models**

Item	Ave. of absolute difference in displacement		Max. of absolute difference in displacement	
	$u$ in the $x$ axis	$v$ in the $y$ axis	$u$ in the $x$ axis	$v$ in the $y$ axis
Unit	$\mu\text{m}$			
Tensile	0.00179	0.00691	0.00490	0.00909
Bend	0.00090	0.00127	0.00357	0.00308

**Table 5. Comparison of total calculation time**

Load	Method	Calculation time
Tensile	FEM	425 sec
	SDM	3.46 sec
Bend	FEM	425 sec
	SDM	3.46 sec
Shear	FEM	425 sec
	SDM	3.46 sec

Shear	0.00019	0.00038	0.00180	0.00085
-------	---------	---------	---------	---------

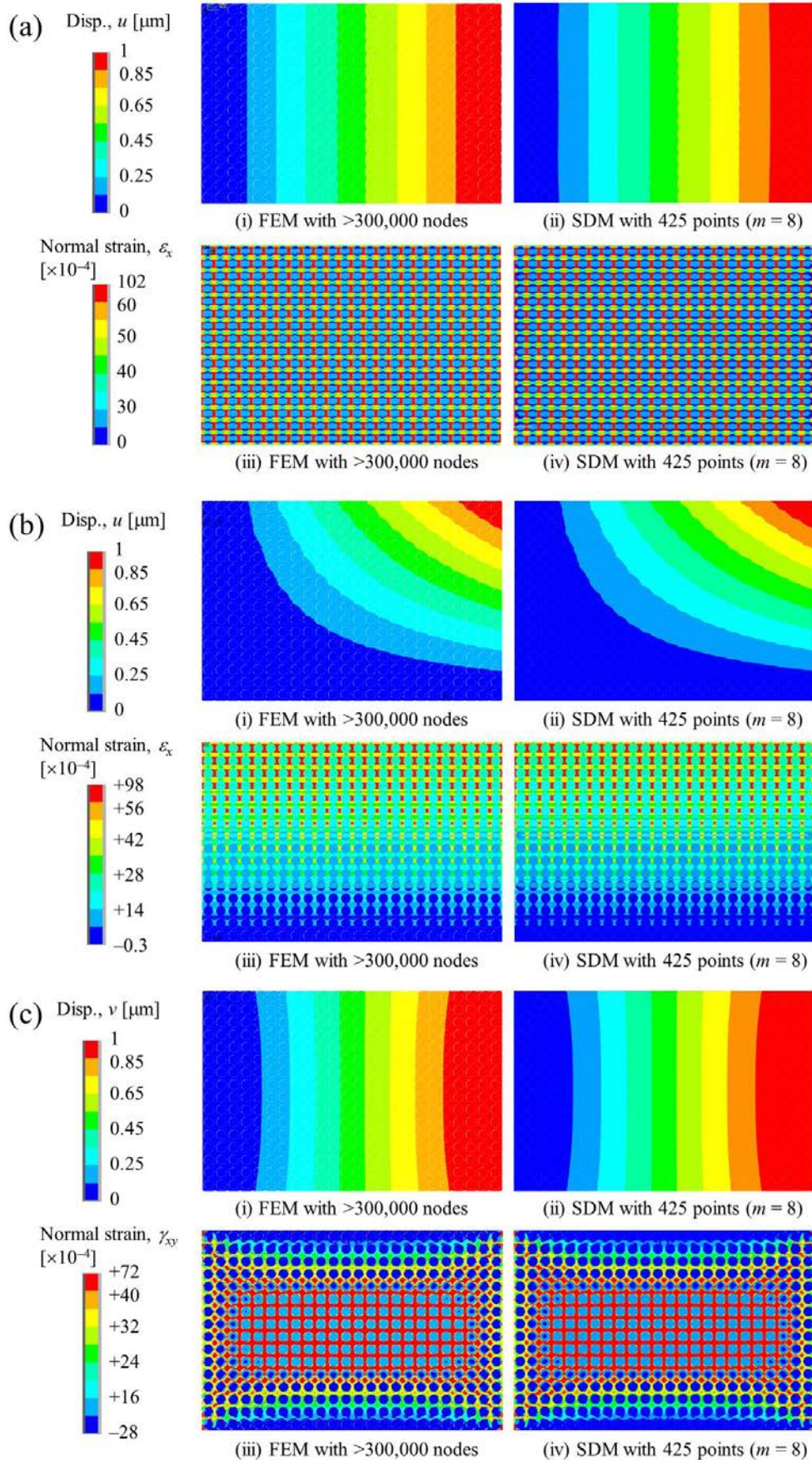


Figure 9. Calculated results of the FRP consisting of simple RVEs when applying: (a) a

**uniaxial tensile load; (b) a bending tensile load; (c) a shearing load.**

## Conclusions

This manuscript proposes a new high-cost-effectiveness multiscale technique, termed the SDM, which is applicable to numerical analyses by modeling a macroscopic field as a “seamless” global domain that has no mesh, grid, cell, or control volume and requires only coarse-grained points. The SDM involves two numerical analyses. The first is an analysis of the local domain to construct accurate interpolating functions and influence coefficients for the second analysis. The second analysis is of the seamless global domain using the special interpolating functions and influence coefficients. There are two novelties of the SDM.

- Dependent-variable distributions interpolated by the special functions satisfy governing equations of the domain almost exactly.
- The seamless domain can enhance continuity of the dependent variable and its gradient.

Therefore, an accurate global solution of the entire field can be obtained by the SDM. This paper explains theoretical aspects of the SDM that are useful in the analysis of domains with a strong boundary effect, anisotropic fields, and heterogeneous materials, as well as isotropic homogenous fields. The analytical precision and computational cost of the SDM technique were investigated for two numerical example problems of two-dimensional periodic heterogeneous materials: stationary temperature field; linear elastic fields. The SDM models with eight reference points (i.e.,  $m = 8$ ) gave much more exact solutions in both example problems than the ordinal FEM.

As a result of the steady-state heat conduction analysis, the average differences in temperature,  $u$ , and temperature gradients,  $\partial u/\partial x$  and  $\partial u/\partial y$ , between the solution of the SDM model represented by only 117 points and that of the conventional FEM model with 20 thousand nodes were  $4.17 \times 10^{-5}$  °C, 0.0305 °C/m, and 0.00649 °C/m, respectively. The temperature and its gradient were highly continuous over the entire material. This verified the feasibility of the SDM for a scalar temperature field. The ordinal FEM required 7.1 times the calculation cost of the SDM in producing a solution as accurate as that of the SDM.

Additionally, we also applied the SDM for linear elastic analysis of vector displacement fields. As a result, the SDM with 117 points provided as accurate solutions as those from conventional FEM using more than 300 thousands of nodes. For all the elastic examples, the average difference of displacement between the SDM solution and the FEM solution with respect to the maximum displacement was less than 0.7 %. The displacement and strain were sufficiently continuous throughout the entire global domains. The SDM solutions were shear-locking-free and hourglass-free because the global domains maintain high analytical resolution and the displacement distributions were flexible enough to fit the true ones. The FEM required more than 100 times the computational cost of the SDM in generating a solution at the same level of accuracy as that of the SDM.

## References

- Wang D, Chen JS. (2006) A locking-free meshfree curved beam formulation with the stabilized conforming nodal integration conforming nodal integration. *Comput Mech* **39**, 83–90.
- Li S, Hao W, Liu WK. (2000) Numerical simulations of large deformation of thin shell structures using meshfree methods. *Comput Mech*; **25**, 102–116.
- Joldes GR, Wittek A, Miller K. (2008) An efficient hourglass control implementation for the uniform strain hexahedron using the Total Lagrangian formulation. *Commun Numer Meth Engng* **24**, 1315–1323.
- Chua J, Efendiev Y, Ginting V, Hou TY. (2008) Flow based oversampling technique for multiscale finite element methods. *Advances in Water Resources* **31(4)**, 599–608.
- Ilic S, Hackl K. (2009) Application of the multiscale FEM to the modeling of nonlinear multiphase materials. *J Theor Appl Mech* **47(3)**, 537–551.

- Jenny P, Lee SH, Tchelepi HA. (2004) Adaptive multiscale finite-volume method for multiphase flow and transport in porous media. *Multiscale Mode. Simul* **3(1)**, 50–64.
- Lunati I, Jenny P. (2006) Multiscale finite-volume method for compressible multiphase flow in porous media. *Journal of Computational Physics* **216(2)**, 616–636.
- Kaczmarczyk Ł, Pearce CJ, Bićanić N. (2010) Studies of microstructural size effect and higher-order deformation in second-order computational homogenization. *Comput Struct* **88(23–24)**, 1383–1390.
- Henning P, Peterseim D. (2013) Oversampling for the multiscale finite element method. *arXiv(mathe NA)* arXiv:1211.5954.
- Efendiev Y, Galvis J, Li G, Presho M. (2013) Generalized multiscale finite element methods. Oversampling strategies. *arXiv(mathe NA)* arXiv:1304.4888.
- Suzuki Y, Soga K, Nakamura Y. (2014) Seamless domain method: a meshfree multiscale numerical analysis. *Int J Numer Meth Eng* (under review).
- Rupnowski P, Gentz M, Sutter JK, Kumosa M. (2005) An evaluation of the elastic properties and thermal expansion coefficients of medium and high modulus graphite fibers. *Composites Part A* **36(3)**: 327–338.